analytical chemistry

pubs.acs.org/ac Article

Electrochemiluminescence Biosensor Based on Entropy-Driven Amplification and a Tetrahedral DNA Nanostructure for miRNA-133a Detection

Linying Yu, Liping Zhu, Mengxia Yan, Sinuo Feng, Jianshe Huang,* and Xiurong Yang*

Cite This: *Anal. Chem.* 2021, 93, 11809−11815 Read Online

ACCESS | Metrics & More | Article Recommendations | Supporting Information

ABSTRACT: The early and rapid diagnosis of acute myocardial infarction (AMI) is of great significance to its treatment. Here, we developed an electrochemiluminescence biosensor based on an entropy-driven strand displacement reaction (ETSD) and a tetrahedral DNA nanostructure (TDN) for the detection of the potential AMI biomarker microRNA-133a. In the presence of the target, numerous $Ru(bpy)_3^{2+}$-labeled signal probes (SP) were released from the preformed three-strand complexes through the process of ETSD. The ETSD reaction cycle greatly amplified the input signal of the target. The released SP could be captured by the TDN-engineered biosensing interface to generate a strong ECL signal. The rigid structure of TDN could significantly improve the hybridization efficiency. With the assistant of double amplification of TDN and ETSD, the developed biosensor has a good linear response ranging from 1 fM to 1 nM for microRNA-133a, and the detection limit is 0.33 fM. Additionally, the constructed biosensor has excellent repeatability and selectivity, demonstrating that the biosensor possesses a great application prospect in clinical diagnosis.

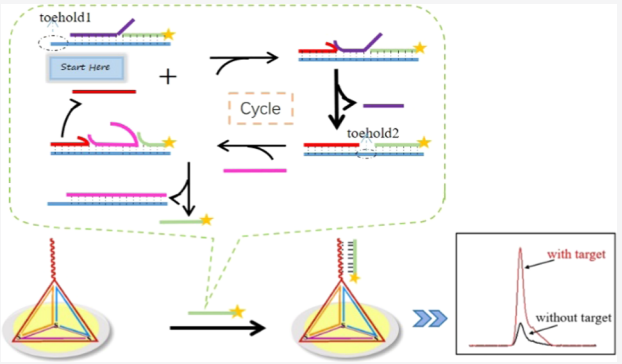

As a serious cardiovascular disease, acute myocardial infarction (AMI) has high incidence and mortality,[1,2] and the morbidity population has gradually become younger in recent years.[3,4] Therefore, its diagnosis and treatment have attracted increasing attention.[5−7] Due to high specificity, cardiac troponin I (cTnI) is considered a "gold standard" for AMI diagnosis.[8−10] However, the high cost of immunoassays and the easy inactivation of antibodies limit its use.[11] It has been reported that the concentration of microRNA-133a (miRNA-133a) in plasma increases sharply after the onset of AMI, and the peak expression of miRNA-133a and cTnI appear almost at the same time.[12,13] Thus, miRNA-133a is also considered an important biomarker for the detection of AMI. However, microRNA has unique characteristics such as small size, high sequence similarity among family members, and low abundance.[14,15] Therefore, it is necessary to develop a sensing strategy with high sensitivity and selectivity to achieve accurate detection of miRNA-133a.

At present, a variety of detection techniques, including fluorescence,[16] electrochemistry,[17] chemiluminescence,[18] electrochemiluminescence (ECL),[19] and so on, have been developed for miRNA detection. Compared with other methods, ECL has attracted extensive attention due to its advantages such as high sensitivity and a wide detection range.[20,21] But DNA-based ECL biosensors usually require nucleic acid to be immobilized on the electrode surface. At present, there are mainly three forms of DNA modified on the electrode surface, i.e., single-stranded DNA,[22] hairpin DNA,[23] and three-dimensional DNA structures.[24] However, single-stranded DNA is a nonrigid structure, and therefore, problems such as uneven distribution and entanglement often occur during the fixation process on the electrode, which results in the decrease of binding efficiency.[25] Although the hairpin structure solves the problem of DNA aggregation to a certain extent, there is still a large steric hindrance on the electrode surface compared with that in a homogeneous solution, which reduces the recognition and hybridization rate and results in the decrease of analytical performance.[26] Compared with the above two methods, a tetrahedral DNA nanostructure (TDN) has attracted great attention due to its simple synthesis, high mechanical rigidity, and structural stability.[27,28] A TDN-engineered biosensing interface can not only adjust the distance between the probes and improve the accessibility of the probes but also reduce nonspecific adsorption on the electrode surface.[29] In addition, because TDN is a three-

Received: June 4, 2021
Accepted: August 9, 2021
Published: August 17, 2021

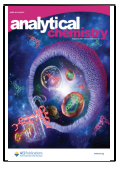

https://doi.org/10.1021/acs.analchem.1c02361
Anal. Chem. 2021, 93, 11809−11815

Scheme 1. Schematic Illustration of (A) the ETSD Amplification Process and (B) the Process of Electrode Surface Modification

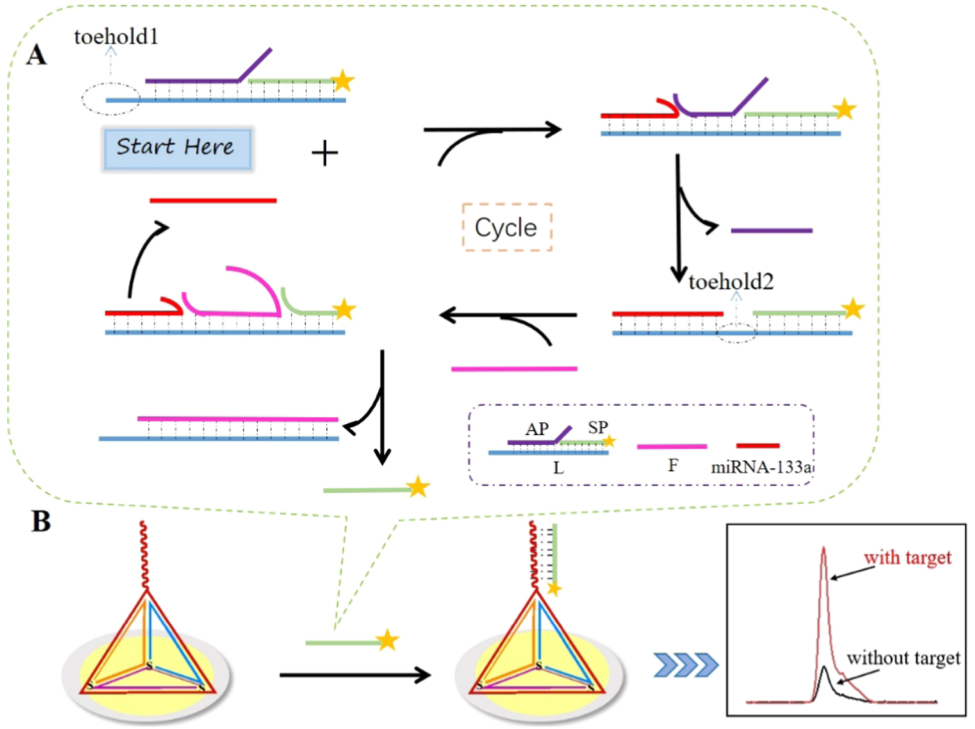

dimensional structure, the probe can be exposed to the solution to have hybridization efficiency similar to that of a homogeneous solution,[30] which further improves the sensitivity of detection.

Due to the low abundance of circulating miRNA, its detection usually requires the introduction of signal amplification technology to improve detection sensitivity.[31] Entropy-driven toehold-mediated strand displacement (ETSD) is an isothermal and enzyme-free amplification process.[32] By adding the target and fuel DNA to the triple-stranded DNA, the signal probe can be output by a simple one-step operation and realize the cyclic amplification of the target.[33] In addition, the double-stranded waste is generated after the reaction, which makes the reaction irreversible, thereby avoiding the interference of the complex environment and increasing the stability of this reaction.[34] Furthermore, the amplification process is driven by the increase of entropy and it has excellent discriminating ability toward single-base mutations according to the difference in the base pair breathing rate.[35,36] Therefore, it has excellent selectivity for the target detection.

Based on the above advantages of TDN and ETSD, a sensitive ECL biosensor was developed for miRNA-133a detection. Scheme 1 displays the specific principle of this biosensor. Three-stranded complexes (S) were formed by a simple annealing process with the linker strand (L), assistant probe (AP), and signal probe (SP). When the target RNA was present, it could hybridize with the single-stranded part of S (toehold 1). From which the AP stand was released and toehold 2 was exposed. Then, the fuel strand (F) could bind to toehold 2, consequently leading to the release of target RNA and $Ru(bpy)_3^{2+}$-labeled signal probes. The released miRNA would trigger a new cycle and release more signal probes, achieving the target cycling amplification. The TDN was designed with a pendant capturing probe at one apex and three thiol groups at other apexes. A biosensing interface was engineered via self-assembly of TDN on gold nanoparticles deposited on a glassy carbon electrode (GCE). The released SPs were captured by the capturing probe, and an amplified ECL signal could be obtained. The ECL intensity was related to the concentration of miRNA-133a. Based on the dual amplification strategy, quantitative detection of the target miRNA-133a could be achieved.

EXPERIMENTAL SECTION

Preparation of TDN. TDN was assembled following the simple annealing technique.[37] DNA sequences are shown in Table S1. Thiolated DNA strands were treated by 2 mM TCEP for 30 min at 37 °C to reduce disulfide bonds before use. In brief, N1 (capturing probe) and thiolated DNA strands (N2, N3, and N4) were dispersed in TM buffer (10 mM Tris-HCl, 50 mM $MgCl_2$, pH 7.4), separately. Then, equimolar quantities of four strands were mixed together. Afterward, the resulting mixture was annealed at 95 °C for 5 min and cooled down to 4 °C rapidly to form a stable TDN.

Entropy-Driven Strand Displacement Reaction. At first, all oligonucleotides (L, AP, SP, and F) were dissolved in TNM buffer (10 mM Tris-HCl, 50 mM NaCl, 10 mM $MgCl_2$, pH 7.4), separately, to obtain the stock solutions. Then, equal volumes of L, AP, and SP with the same concentration were mixed together with a final concentration of 2.5 μM. Subsequently, the obtained mixture was denatured at 95 °C for 5 min and then cooled down to 25 °C at a rate of 0.6 °C/min to form a three-strand DNA complex. Then, different concentrations of the target sequence and F were mixed with the three-strand DNA complex and incubated at 25 °C for 2 h.

Fabrication of the ECL Biosensor and ECL Measurement. The bare GCE was pretreated according to the reported

https://doi.org/10.1021/acs.analchem.1c02361
Anal. Chem. 2021, 93, 11809−11815

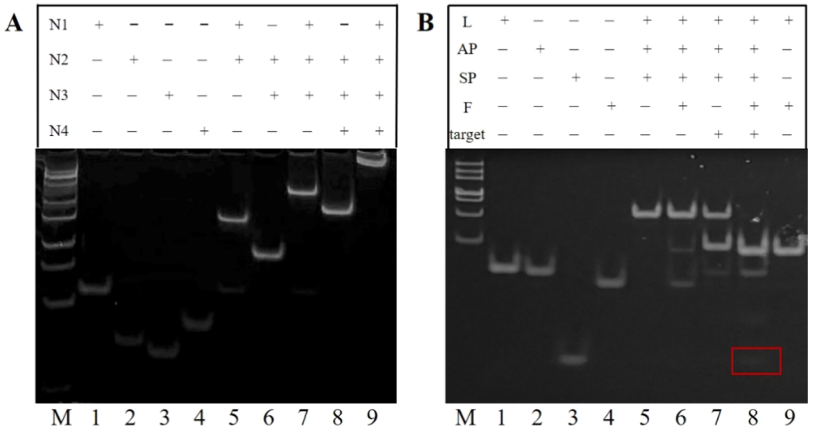

Figure 1. (A) PAGE characterization of TDN. M: DNA marker; lanes 1−4: N1, N2, N3, and S4; lanes 5−8: N1 + N2, N2 + N3, N1 + N2 + N3, and N2 + N3 + N4; lane 9: N1 + N2 + N3 + N4. (B) PAGE image of ETSD products. M: DNA marker; lane 1: L; lane 2: AP; lane 3: SP; lane 4: F; lane 5: S (L + AP + SP); lane 6: S + F; lane 7: S + target; lane 8: S + F + target; and lane 9: L + F.

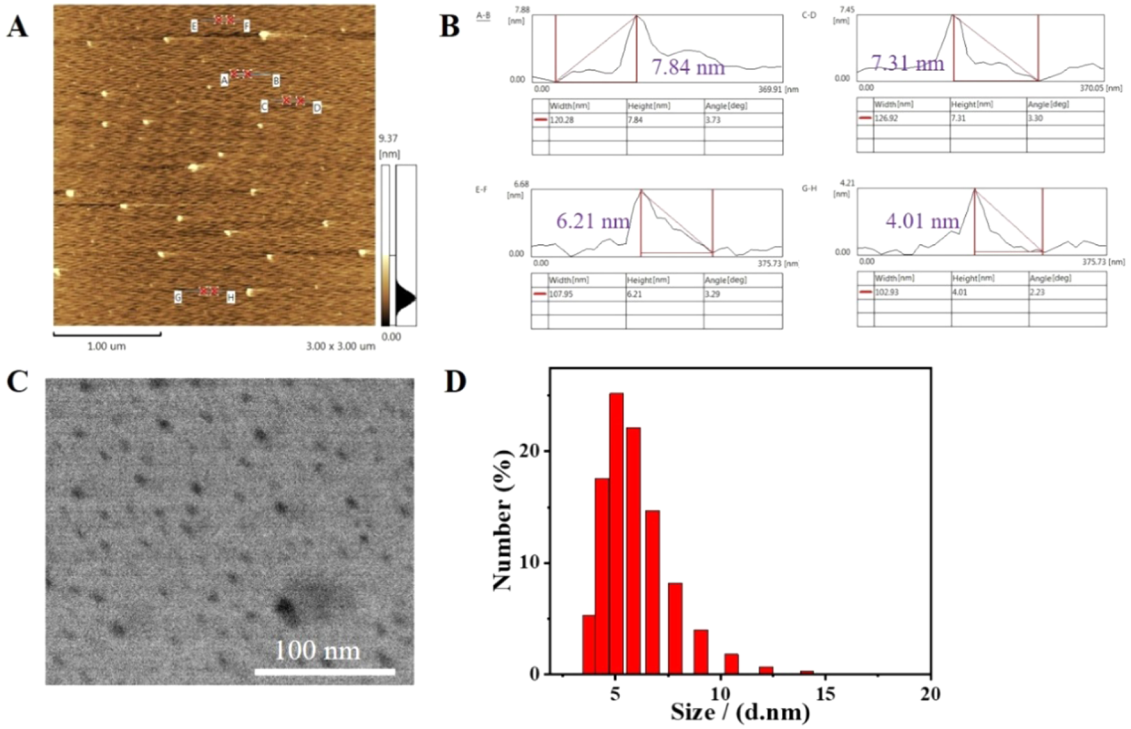

Figure 2. (A) AFM Characterization of TDN. (B) The height of the TDN marked in (A). (C) TEM image of TDN. (D) DLS size distribution of TDN.

literature.[37] The obtained GCE was immersed in a 1% $HAuCl_4$ solution to electrodeposit AuNPs at −0.2 V for 30 s and then cleaned with ultrapure water. Afterward, the AuNPs/GCE was incubated overnight with 8 μL of the TDN solution at 4 °C and then rinsed three times with PBS buffer (0.1 M KCl, pH 7.4). Next, the modified electrode was further incubated with 10 μL of the ETSD reaction solution at 25 °C and cleaned with PBS buffer for the next step experiment. Ultimately, the ECL signals were measured in 5 mL of PBS buffer containing 25 mM DBAE. The potential was swept from 0 to 1.2 V with a scan rate of 0.1 V/s, and throughout the experiment, the photomultiplier tube (PMT) voltage was set to 800 V.

Polyacrylamide Gel Electrophoresis (PAGE). A 12% polyacrylamide gel was employed for the analysis of the DNA hybridization products in TBE buffer (89 mM Tris-boric acid, 2 mM EDTA, pH 8.4). Ten microliters of the sample was mixed with DNA-loading buffer (6×) before being loaded onto the gel. The electrophoresis of the TDN sample was carried out at 120 V for 110 min. The gel electrophoresis analysis of ETSD was performed at 80 V for 80 min. Subsequently, the gel was stained with the GelRed solution for 30 min and imaged under an ultraviolet lamp.

RESULTS AND DISCUSSION

Characterization of TDN. To verify the successful formation of TDN, we characterized TDN by PAGE, atomic force microscopy (AFM), transmission electron microscopy (TEM), and dynamic light scattering (DLS). Figure 1A shows that the PAGE bands in lanes 1, 2, 3, and 4 correspond to N1, N2, N3, and N4. The bands in lanes 5−8 represent the

https://doi.org/10.1021/acs.analchem.1c02361
Anal. Chem. 2021, 93, 11809−11815

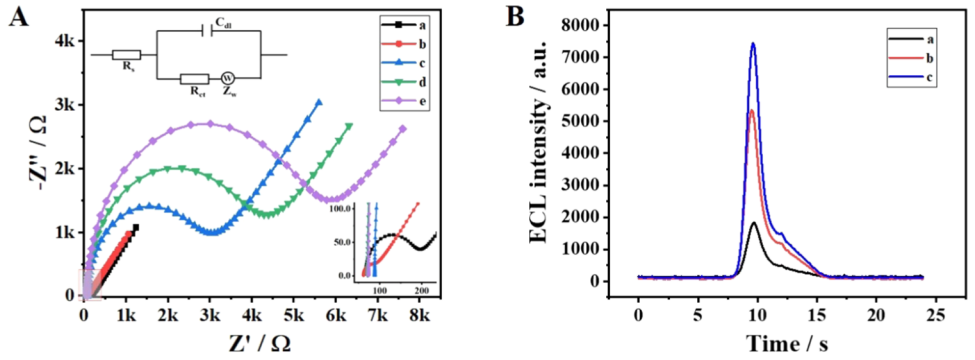

Figure 3. (A) EIS curves of the electrodes: (a) GCE, (b) depAu/GCE, (c) TDN/depAu/GCE, (d) ETSD product (10 pM target) incubated TDN/depAu/GCE, and (e) ETSD product (1 nM target) incubated TDN/depAu/GCE. (B) ECL response to miRNA-133a: (a) 0, (b) 10 pM, and (c) 1 nM.

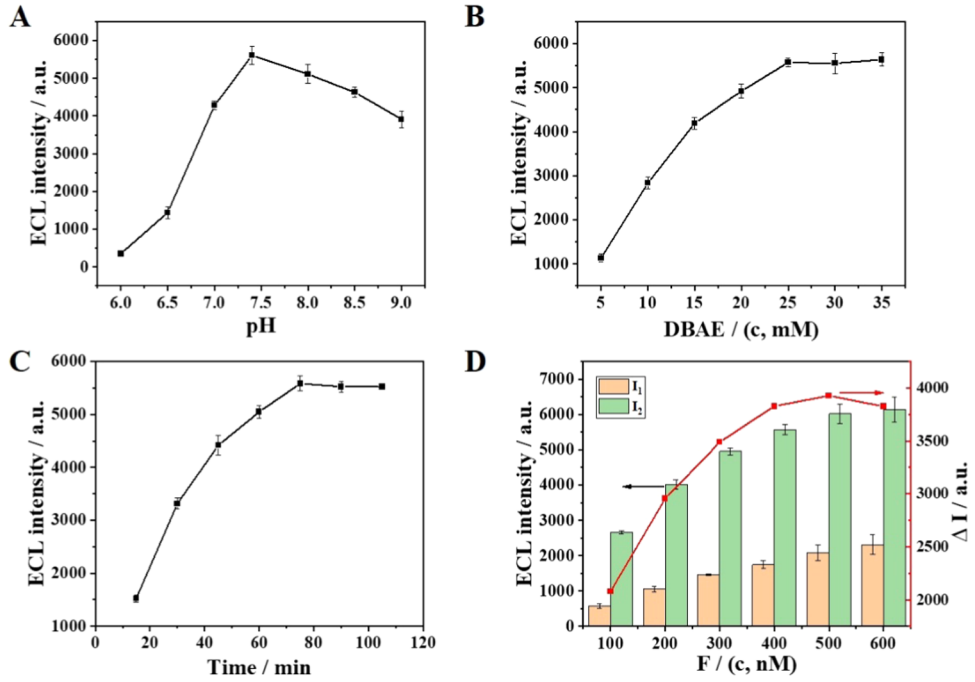

Figure 4. Optimization of (A) pH, (B) the concentration of DBAE, (C) the incubation time between TDN and the strand displacement product, and (D) the concentration of *F*. The concentration of miRNA-133a was 10 pM.

products formed by direct annealing two or three strands among N1, N2, N3, and N4. The slower migration rate demonstrated the successful formation of hybridization products between them. The assembled products of N1, N2, N3, and N4 showed the slowest migration rate (lane 9), which was consistent with the expected results. The AFM image (Figure 2A) showed that the size of TDN ranged from 4.01 to 7.84 nm (Figure 2B), which was close to the theoretical height (5.02 nm). TEM characterization (Figure 2C) showed that TDN had uniform size distribution (6.15 ± 0.46 nm), and DLS (Figure 2D) showed that the average hydrodynamic diameter of TDN was 5.87 nm. All these results prove that TDN was successfully synthesized.

PAGE Characterization of ETSD. The feasibility of ETSD was also proved by PAGE. As displayed in Figure 1B, lanes 1−4 correspond to L (3 μM), AP (3 μM), SP (7 μM), and F (3 μM). A new band appeared in lane 9 when L and F were mixed, proving that the L/F duplex was formed. Lane 5 was a mixture (1.5 μM) of L, AP, and SP, and only a bright single band was observed. This proved the successful formation of a triple-stranded DNA complex (S). Compared with lane 5, a very weak band appeared in the same region as the L/F duplex in lane 6, demonstrating that the ignorable leakage in this system was induced by the direct addition of the F strand. However, after adding the target to S, lane 7 in the PAGE image shows a bright band appearing above the L/F duplex region accompanied by the weakened S band. This result suggested that the AP chain in S was replaced by the target, and a new triple-stranded complex (L/target/SP) formed. When both the target and F were mixed with S, a large number of L/F duplex appeared in lane 8 with obvious AP and SP. All these results proved that the target-induced amplification reaction has been successfully designed.

EIS and ECL Characterization. The step-by-step modification process of the biosensor was characterized by electrochemical impedance spectroscopy (EIS). As shown in Figure 3A, the EIS of the bare GCE shows a small semicircle diameter (curve a). After the Au nanoparticles were deposited on the GCE (depAu/GCE), EIS became a straight line (curve b), which was attributed to the good conductivity and large

https://doi.org/10.1021/acs.analchem.1c02361
Anal. Chem. 2021, 93, 11809−11815

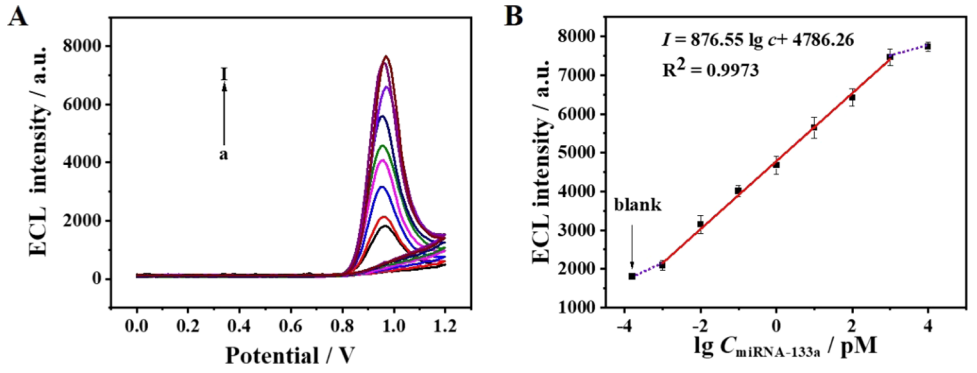

Figure 5. (A) ECL intensity versus potential curves. The concentration of miRNA-133a was a to I: 0 fM, 1 fM, 10 fM, 100 fM, 1 pM, 10 pM, 100 pM, 1 nM, and 10 nM. (B) The calibration plots of the ECL biosensor.

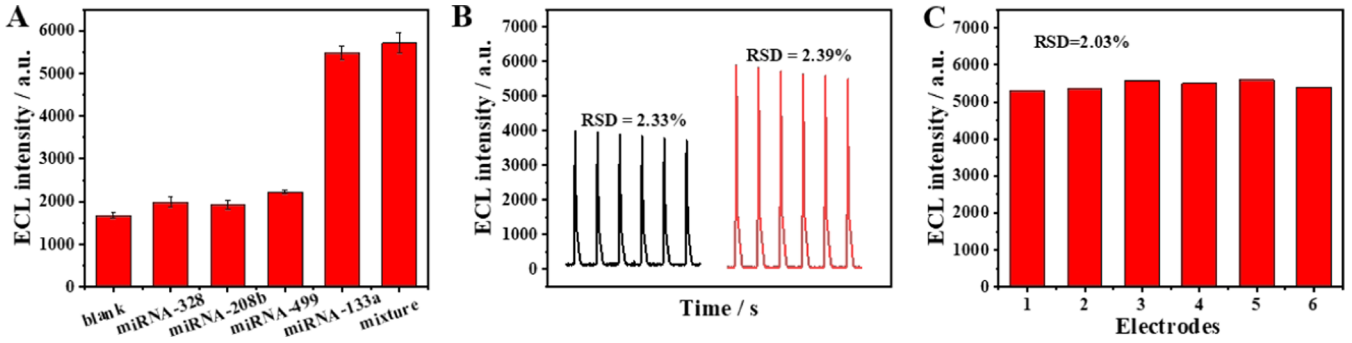

Figure 6. (A) Selectivity evaluation of the constructed biosensor. All of the concentration of RNA was 10 pM. (B) Stability of the ECL biosensor with two concentrations of miRNA-133a (100 fM and 10 pM). (C) Repeatability assays of the ECL biosensor for 10 pM miRNA-133a.

surface of the gold nanoparticles. The electron-transfer resistance (Ret) increased significantly after TDN was modified on the electrode surface (curve c). This is because of the electrostatic repulsion between negatively charged DNA and the $[Fe(CN)_6]^{3-/4-}$ redox probe, which impeded the electron transfer. The Ret showed an increasing trend after the biosensor was incubated with the strand displacement product (curves d and e), and the higher the concentration of the target, the larger the Ret. These results are consistent with expectations, confirming the successful development of the biosensor.

To further evaluate the feasibility of the experiment, the ECL response of the constructed biosensor to the target RNA was tested. From Figure 3B we can observe that a low background signal was detected in the absence of miRNA-133a, which was possibly caused by the partial leakage of the displacement reaction. However, the ECL signal was significantly enhanced when the target was present (curves b and c), and as the concentration of the target increased, the ECL signal became stronger, indicating that the constructed biosensor could respond to the target.

Optimization of Assay Conditions. The pH value, the concentration of DBAE, the incubation time between TDN and the strand displacement product (SP), and the concentration of the F strand were optimized to optimize the analysis performance. As displayed in Figure 4A, as the pH changed from 6.0 to 9.0, the ECL signal first increased rapidly and then gradually decreased after reaching the peak at pH 7.4. Thus, pH 7.4 was used as the optimal pH value. The concentration of the coreactant reagent would affect the luminous efficiency. As displayed in Figure 4B, when the concentration of DBAE gradually increased from 5 to 35 mM, the ECL intensity gradually increased and leveled off at 25 mM. Therefore, 25 mM DBAE was selected for the next experiment. The effect of the incubation time between TDN and the strand displacement product (SP) is shown in Figure 4C. By increasing the incubation time from 15 to 105 min, the ECL intensity first increased and reached a stable level at 75 min, indicating that 75 min was the best incubation time. The concentration of F was a key factor because it affected the kinetics of entropy-driven chain displacement reactions. It participated not only in the chain displacement reaction process but also in the side reaction process. Therefore, it is necessary to optimize the F concentration to obtain a high signal-to-background ratio. ΔI, the difference of the ECL intensity between the presence (I_2) and absence of the target (I_1), was used to evaluate the effect of F concentration. As displayed in Figure 4D, ΔI increased as the concentration of F increased, and started to stabilize when the concentration of F was 400 nM. Thus, 400 nM was selected for the following study.

Performance of the ECL Biosensor. The analytical performance of the developed biosensor was evaluated under the optimal conditions. The ECL intensity gradually enhanced as the concentration of the target miRNA-133a increased (Figure 5A), and the ECL intensity has a linear relationship with the logarithm of miRNA-133a concentration within a target concentration range of 1 fM to 1 nM (Figure 5B). The linear equation was $I = 876.55 \lg c + 4786.26$ with a correlation coefficient of 0.9973. The limit of detection (LOD) was 0.33 fM (S/N = 3). The developed biosensor showed a wide detection range and a low detection limit compared with the previously reported RNA detection sensors (Table S2),

https://doi.org/10.1021/acs.analchem.1c02361
Anal. Chem. 2021, 93, 11809−11815

indicating that it has a great application prospect for the detection of miRNA-133a.

Selectivity, Stability, and Reproducibility. To evaluate the selectivity of the constructed biosensor, the ECL response of the biosensor was measured using the RNAs (miRNA-499a, miRNA-208b, and miRNA-328) related to AMI as interfering substances. It can be seen from Figure 6A that under the same conditions, the ECL intensities produced by the interfering RNAs were close to the background intensity, while the target RNA and the mixture of the target RNA and interfering RNAs produced similar and significantly enhanced ECL signals, which confirmed that the biosensor had excellent selectivity to miRNA-133a. Stability was evaluated by measuring the relative standard deviation (RSD) of the ECL signal obtained by scanning continuously for 6 cycles with 100 fM and 10 pM miRNA-133a (Figure 6B). The RSD was 2.33 and 2.39%, respectively, indicating that the constructed biosensor had excellent stability. In addition, the fabrication reproducibility was evaluated by measuring the 10 pM target with six electrodes, and the calculated RSD was 2.03% (Figure 6C), indicating that the biosensor had excellent reproducibility.

Detection of miRNA-133a in Human Serums. The practical use of the constructed biosensor was evaluated by measuring the ECL response signals of 1, 10, and 100 pM miRNA-133a in 5 and 10% human serum samples by the standard addition method. The recovery was in the range of 95.60−110.91%, and the RSD was in the range of 0.87−4.06% (Table S3). It showed that the constructed biosensor had a promising application for miRNA detection in real samples.

CONCLUSIONS

In summary, a highly sensitive and selective ECL biosensor based on TDN and the entropy-driven chain displacement reaction was constructed. The proposed biosensor possesses the following merits. First, the TDN-engineered biosensing interface provided a controllable surface spacing between capturing probes, which could reduce the entanglement between the probes and improved the hybridization efficiency. Second, TDN could reduce the nonspecific adsorption of nucleic acids on the electrode surface, thereby avoiding the blocking process and simplifying the construction step of the biosensor. Third, the entropy-driven chain displacement reaction could achieve the cyclic amplification of the target and improved the detection sensitivity. Thanks to these advantages, the developed biosensor showed high sensitivity and a wide detection range for miRNA-133a detection, as well as excellent selectivity and reproducibility. The proposed ECL biosensor would provide a promising alternative method for miRNA or other nucleic acid detection.

ASSOCIATED CONTENT

Supporting Information

The Supporting Information is available free of charge at https://pubs.acs.org/doi/10.1021/acs.analchem.1c02361.

Reagents, apparatus, and sequences of oligonucleotides used in this study (Table S1); comparison of the analytical results of the proposed biosensor for miRNA-133a detection with previously reported strategies (Table S2); and recovery for miRNA-133a detection in real human serum (Table S3) (PDF)

AUTHOR INFORMATION

Corresponding Authors

Jianshe Huang − *State Key Laboratory of Electroanalytical Chemistry, Changchun Institute of Applied Chemistry, Chinese Academy of Sciences, Changchun, Jilin 130022, China*; Phone: +86 431 85262964; Email: huangjs@ciac.ac.cn; Fax: +86 431 85689278

Xiurong Yang − *State Key Laboratory of Electroanalytical Chemistry, Changchun Institute of Applied Chemistry, Chinese Academy of Sciences, Changchun, Jilin 130022, China; University of Science and Technology of China, Hefei, Anhui 230026, China*; orcid.org/0000-0003-0021-5135; Phone: +86 431 85262056; Email: xryang@ciac.ac.cn; Fax: +86 431 85689278

Authors

Linying Yu − *State Key Laboratory of Electroanalytical Chemistry, Changchun Institute of Applied Chemistry, Chinese Academy of Sciences, Changchun, Jilin 130022, China; University of Science and Technology of China, Hefei, Anhui 230026, China*

Liping Zhu − *University of Science and Technology of China, Hefei, Anhui 230026, China*

Mengxia Yan − *State Key Laboratory of Electroanalytical Chemistry, Changchun Institute of Applied Chemistry, Chinese Academy of Sciences, Changchun, Jilin 130022, China; University of Science and Technology of China, Hefei, Anhui 230026, China*

Sinuo Feng − *State Key Laboratory of Electroanalytical Chemistry, Changchun Institute of Applied Chemistry, Chinese Academy of Sciences, Changchun, Jilin 130022, China; University of Science and Technology of China, Hefei, Anhui 230026, China*

Complete contact information is available at: https://pubs.acs.org/10.1021/acs.analchem.1c02361

Author Contributions

The manuscript was written through contributions of all authors.

Notes

The authors declare no competing financial interest.

ACKNOWLEDGMENTS

This work was supported by the National Natural Science Foundation of China (Nos. 22034006, 21627808, and 21721003), the Key Research Program of Frontier Sciences, CAS (QYZDY-SSW-SLH019), and the National Key Research and Development Program of China (2016YFA0201301).

REFERENCES

(1) Reed, G. W.; Rossi, J. E.; Cannon, C. P. *Lancet* **2017**, *389*, 197−210.
(2) Barnett, R. *Lancet* **2019**, *393*, 2580.
(3) Guo, X. F.; Li, Z.; Vittinghoff, E.; Sun, Y. X.; Pletcher, M. J. *Nat. Rev. Cardiol.* **2018**, *15*, 119.
(4) Gulati, R.; Behfar, A.; Narula, J.; Kanwar, A.; Lerman, A.; Cooper, L.; Singh, M. *Mayo Clin. Proc.* **2020**, *95*, 136−156.
(5) Abuzaid, A.; Fabrizio, C.; Felpel, K.; Al Ashry, H. S.; Ranjan, P.; Elbadawi, A.; Mohamed, A. H.; Barssoum, K.; Elgendy, I. Y. *Am. J. Med.* **2018**, *131*, 693−701.
(6) Mora-Ruíz, M. D.; Blanco-Favela, F.; Chavez Rueda, A. K.; Legorreta-Haquet, M. V.; Chavez-Sanchez, L. *Mol. Immunol.* **2019**, *107*, 71−78.

(7) Han, X.; Li, S. H.; Peng, Z. L.; Othman, A. M.; Leblanc, R. *ACS Sens.* **2016**, *1*, 106−114.
(8) Weber, M.; Rau, M.; Madlener, K.; Elsaesser, A.; Bankovic, D.; Mitrovic, V.; Hamm, C. *Clin. Biochem.* **2005**, *38*, 1027−1030.
(9) Chistiakov, D. A.; Orekhov, A. N.; Bobryshev, Y. V. *J. Mol. Cell. Cardiol.* **2016**, *94*, 107−121.
(10) Polanczyk, C. A.; Lee, T. H.; Cook, E. F.; Walls, R.; Wybenga, D.; Printy-Klein, G.; Ludwig, L.; Guldbrandsen, G.; Johnson, P. A. *J. Am. Coll. Cardiol.* **1998**, *32*, 8−14.
(11) Muzyka, K.; Saqib, M.; Liu, Z. Y.; Zhang, W.; Xu, G. B. *Biosens. Bioelectron* **2017**, *92*, 241−258.
(12) Wang, C.; Jiang, Q. *Acta Pharmacol. Sin.* **2018**, *39*, 1110−1119.
(13) D'Alessandra, Y.; Devanna, P.; Limana, F.; Straino, S.; Di Carlo, A.; Brambilla, P. G.; Rubino, M.; Carena, M. C.; Spazzafumo, L.; De Simone, M.; Micheli, B.; Biglioli, P.; Achilli, F.; Martelli, F.; Maggiolini, S.; Marenzi, G.; Pompilio, G.; Capogrossi, M. C. *Eur. Heart J.* **2010**, *31*, 2765−2773.
(14) Zhu, L.; Ye, J.; Wang, S.; Yan, M. X.; Zhu, Q. J.; Huang, J. S.; Yang, X. Y. *Chem. Commun.* **2019**, *55*, 11551−11554.
(15) Dong, H.; Lei, J. P.; Ding, L.; Wen, Y. Q.; Ju, H. X.; Zhang, X. J. *Chem. Rev.* **2013**, *113*, 6207−6233.
(16) Li, D.; Zhou, W. J.; Yuan, R.; Xiang, Y. *Anal. Chem.* **2017**, *89*, 9934−9940.
(17) Zhu, J.; Gan, H. Y.; Wu, J.; Ju, H. X. *Anal. Chem.* **2018**, *90*, 5503−5508.
(18) Sun, Y.; Shi, L.; Wang, Q. W.; Mi, L.; Li, T. *Anal. Chem.* **2019**, *91*, 3652−3658.
(19) Yang, J.; Dou, B. T.; Yuan, R.; Xiang, Y. *Anal. Chem.* **2017**, *89*, 5138−5143.
(20) Hu, L.; Xu, G. B. *Chem. Soc. Rev.* **2010**, *39*, 3275−3304.
(21) Liu, Z.; Qi, W. J.; Xu, G. B. *Chem. Soc. Rev.* **2015**, *44*, 3117−3142.
(22) Deng, H.-M.; Huang, L. J.; Chai, Y. Q.; Yuan, R.; Yuan, Y. L. *Anal. Chem.* **2019**, *91*, 2861−2868.
(23) Huo, X.-L.; Zhang, N.; Yang, H.; Xu, J. J.; Chen, H. Y. *Anal. Chem.* **2018**, *90*, 13723−13728.
(24) Lu, N.; Pei, H.; Ge, Z. L.; Simmons, C. R.; Yan, H.; Fan, C. H. *J. Am. Chem. Soc.* **2012**, *134*, 13148−13151.
(25) Li, M.-J.; Zheng, Y. N.; Liang, W. B.; Yuan, R.; Chai, Y. Q. *ACS Appl. Mater. Interfaces* **2017**, *9*, 42111−42120.
(26) Ren, R.; Bi, Q.; Yuan, R.; Xiang, Y. *Sens. Actuators, B* **2020**, *304*, No. 127068.
(27) Lu, J.; Wang, J.; Hu, X. L.; Gyimah, E.; Yakubu, S.; Wang, K.; Wu, X. Y.; Zhang, Z. *Anal. Chem.* **2019**, *91*, 7353−7359.
(28) Su, J.; Wu, F. B.; Xia, H. P.; Wu, Y. F.; Liu, S. Q. *Chem. Sci.* **2020**, *11*, 80−86.
(29) Pei, H.; Lu, N.; Wen, Y. L.; Song, S. P.; Liu, Y.; Yan, H.; Fan, C. H. *Adv. Mater.* **2010**, *22*, 4754−4758.
(30) Wen, Y. L.; Li, L. Y.; Li, J.; Lin, M. H.; Liu, G.; Liang, W.; Xu, L.; Li, Y.; Zuo, X. L.; Ren, S. Z.; Zhu, Y. *Anal. Chem.* **2020**, *92*, 4498−4503.
(31) Zhou, H.; Liu, J.; Xu, J. J.; Zhang, S. S.; Chen, H. Y. *Chem. Soc. Rev.* **2018**, *47*, 1996−2019.
(32) Zhang, Y.; Wang, W. J.; Lin, Z. Y.; Liu, B.; Zhou, X. *Biosens. Bioelectron.* **2020**, *161*, 112256.
(33) Li, S. K.; Liu, Z. T.; Li, J. Y.; Chen, A. Y.; Chai, Y. Q.; Yuan, R.; Zhuo, Y. *ACS Appl. Mater. Interfaces* **2018**, *10*, 14483−14490.
(34) Zhang, N.; Shi, X. M.; Guo, H. Q.; Zhao, X. Z.; Zhao, W. W.; Xu, J. J.; Chen, H. Y. *Anal. Chem.* **2018**, *90*, 11892−11898.
(35) Zhang, X. L.; Yang, Z. H.; Chang, Y. Y.; Liu, D.; Li, Y. R.; Chai, Y. Q.; Zhuo, Y.; Yuan, R. *Chem. Sci.* **2020**, *11*, 148−153.
(36) Lv, Y.; Cui, L.; Peng, R.; Zhao, Z.; Qiu, L.; Chen, H.; Jin, C.; Zhang, X. B.; Tan, W. *Anal. Chem.* **2015**, *87*, 11714−11720.
(37) Ye, J.; Zhu, L. P.; Yan, M. X.; Zhu, Q. J.; Lu, Q. Q.; Huang, J. S.; Cui, H.; Yang, X. R. *Anal. Chem.* **2019**, *91*, 1524−1531.

https://doi.org/10.1021/acs.analchem.1c02361
Anal. Chem. 2021, 93, 11809−11815